

Revealing Secondary Particle Signatures in PoCA-Based Muography

Rongfeng Zhang,¹ Zibo Qin,¹ Cheng-en Liu,¹ Qite Li,^{1, a)} Yong Ban,¹ Chen Zhou,¹ and Qiang Li^{1, b)}
*State Key Laboratory of Nuclear Physics and Technology, School of Physics, Peking University
 Beijing, 100871, China*

This manuscript has been submitted to the Journal of Applied Physics for consideration.

(Dated: 8 July 2025)

This work reinterprets so-called ‘noise’ in cosmic ray imaging, demonstrating that reconstructed Points of Closest Approach (PoCA points) at the detector locations contain valuable physical information that has been traditionally disregarded. Through comprehensive analysis of data from the detection system of four resistive plate chambers (RPCs) and Monte Carlo simulations employing energy deposition weighting for coordinate determination, we establish that these points physically originate from secondary particles produced by cosmic ray interactions with materials of both detectors and surrounding structures. The research yields two principal findings: first, the generation of secondary particles significantly affects the measurement accuracy of cosmic ray positions; second, the roof structure significantly impacts the distribution of PoCA points at detector positions, where quantitative analysis demonstrates a strong correlation between roof thickness and the number of reconstructed PoCA points — a relationship that can be precisely measured through z -coordinate distribution analysis in specific intervals. These discoveries demonstrate that the same detection system can extract information from a new dimension, enabling acquisition of more comprehensive physical results. More importantly, it suggests the necessity to revise standard analysis approaches to fully exploit this additional information channel in cosmic ray tomography.

I. INTRODUCTION

Muon tomography was first proposed in 2003¹, with the PoCA algorithm representing one of the most widely used methods. The imaging principle relies on Coulomb scattering of cosmic ray muons, assuming each muon’s scattering occurs at a single point corresponding to the closest approach between its incoming and outgoing trajectories.² Each PoCA point is weighted according to its deflection angle, where larger scattering angles receive higher weights due to their stronger correlation with high-density materials. Object images are obtained through pixel-based reconstruction.

In practical cosmic ray imaging applications, the naturally occurring cosmic ray flux (comprising both muons and hadronic components) is typically utilized rather than purified muon beams. Recent advances in PoCA-based imaging research have primarily developed along two parallel tracks: (1) enhanced information extraction through innovative detector system designs (Ref.^{3–5}), and (2) improved data processing via theoretical refinements (Ref.^{6,7}) or machine learning approaches (Ref.^{5,8–10}). Conventionally, imaging analyses have focused exclusively on PoCA point distributions within sample regions, while treating points reconstructed in other spatial domains as measurement noise. However, conventional analyses typically discard PoCA points outside the sample volume as noise. This work demonstrates that such points contain physically meaningful signatures, providing an underutilized source of information for muography.

II. EXPERIMENTAL SETUP

This study evolved from the PKMu collaboration’s dark matter search program¹¹, where its initial objective focused on characterizing various experimental noise sources. Consequently, the research maintains the original detection system configuration developed for that purpose. The system comprises four resistive plate chambers (RPCs) arranged with inter-layer spacings of 20 cm, 50 cm, and 20 cm between bottom surfaces (Fig. 1a). Each RPC detects particles through timing measurements.^{12,13} That is, the hit position is reconstructed from the time difference between signals in the orthogonal X and Y directions, while the timing (T) signal provides the trigger. In the study, the detection area is $280 \times 280 \text{ mm}^2$. The triggering logic requires coincident signals either from the top two chambers ($\text{RPC0} \wedge \text{RPC1}$) or bottom two chambers ($\text{RPC2} \wedge \text{RPC3}$) to register a valid event. Due to the requirements of the PoCA algorithm, the data underwent a secondary screening after passing through four layers of RPC during analysis. Using this setup, the experiment collected 63 days of target-free cosmic ray measurements.

III. SIMULATION SETUP

The GEANT4 11.1.2 toolkit^{14–16} performed Monte Carlo simulations, while the PKMu collaboration developed the detector geometry and maintains its open-source implementation on GitHub.¹⁷ The rectangular sensitive area in each detector captures particle type, deposited energy, and spatial coordinates during particle interactions. The energy deposition weighting determines the final coordinates within each sensitive area, with fixed z -positions at 450 mm, 250 mm, -250 mm, and -450 mm. The simulated x and y coordinates are modified by applying random Gaussian offsets based on the experimen-

^{a)}Contact author: liqt@pku.edu.cn

^{b)}Contact author: qliphy0@pku.edu.cn

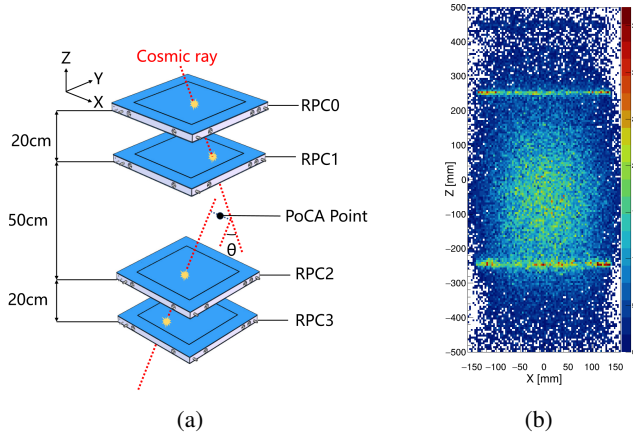


FIG. 1: (a) Detection system. (b) PoCA point distribution in the X-Z direction.

tally determined detector resolution (about $0.7 \text{ mm}(\sigma)$). All simulation data is saved in ROOT format¹⁸ for analysis.

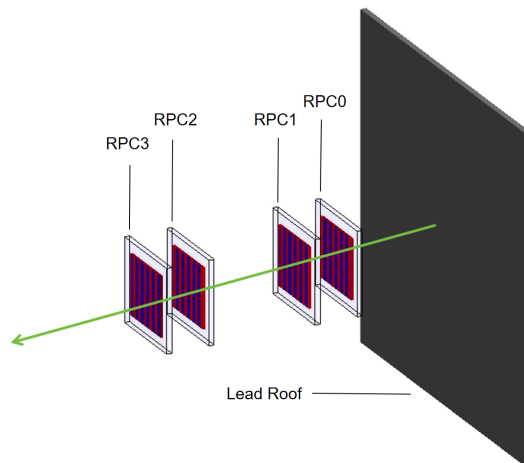


FIG. 2: GEANT4 simulation setup: Lead roof (gray) and detector (white wireframe). The green arrow represents the direction of incident of the particles.

The cosmic-ray showers were generated using the CRY¹⁹ software package, which reproduces the characteristic energy spectrum and angular distributions observed in the Beijing region. The initial simulation configuration employed a $300 \times 300 \text{ mm}^2$ planar particle generator positioned above RPC0. For studies of roof effect, the simulation incorporated lead roof layers of varying thicknesses while maintaining a constant 500 mm separation between RPC0 and the particle generation plane. The dimensions of the roof were matched to the generator area, while the particle plane was enlarged to $1515 \times 1515 \text{ mm}^2$ to ensure unbiased sampling of the incident angles (Fig. 2).

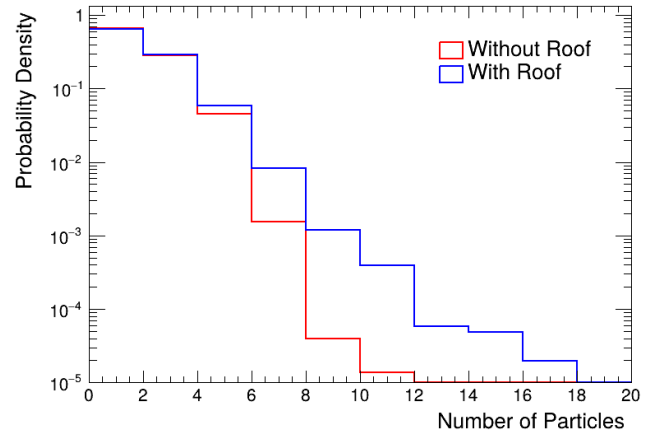


FIG. 3: Normalized particle count distribution in RPC0: Comparison between simulation without roof (red line) and simulation with 50 mm lead roof shielding (blue line).

IV. DATA ANALYSIS

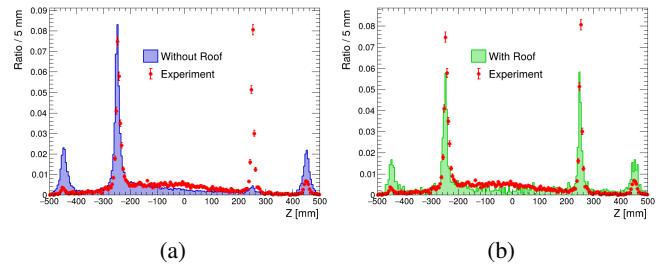


FIG. 4: Experimental and simulated comparison of the filtered PoCA z -distributions. The experimental data is represented by points with error bars. (a) Simulation without roof. (b) Simulation with lead roof of 9 mm thickness.

A. Simulation-experiment discrepancy

The target-free experimental data initially revealed distinct clustering of PoCA points on the detector, as clearly illustrated in the PoCA imaging results (Fig. 1b). To effectively isolate these signals from the cosmic-ray multiple scattering background in air, the analysis employed stringent selection criteria ($\theta > 0.2 \text{ rad}$, $\Delta d < 10 \text{ mm}$, within $300 \times 300 \times 1000 \text{ mm}^3$ volume), where θ represents the scattering angle and Δd represents the spatial separation between the incident and outgoing muon trajectories. A threshold of Δd is applied to ensure that both tracks originate from a common scattering plane. The apparent clustering of PoCA points at the RPC detector layers, as observed in Fig. 1b and Fig. 4a, primarily arises from position mismeasurements caused by secondary particles. When one of the RPC layers registers a displaced hit — typically

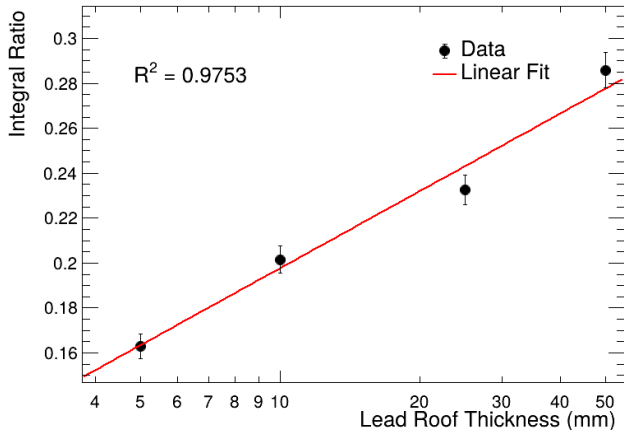


FIG. 5: The correlation between the thickness of lead roofing and the corresponding integral ratios. The error bars represent the statistical uncertainty arising from fluctuations in event counts. The horizontal axis is displayed on a logarithmic scale to emphasize the variations across different thicknesses.

due to secondary particles rather than a muon ray — reconstructed incoming and outgoing tracks deviate from the true trajectory. As a result, the PoCA algorithm interprets this angular deviation as a large-angle Coulomb scattering, and erroneously localizes the scattering point near the detector plane where the mismeasurement occurred. Consequently, these artificial PoCA points accumulate at the RPC positions in the z -coordinate histogram. However, there is a significant discrepancy in the filtered PoCA z -distributions (Fig. 4a). While the experimental data showed pronounced clustering at RPC1’s position, this feature was notably absent in the simulation results.

B. Roof simulations

The systematic difference was investigated through roof simulations. As shown in Fig. 3, the introduction of lead shielding dramatically modifies the particle count distribution in RPC0’s sensitive area, clearly demonstrating the shadowing effect of materials, which cause the millimeter-scale coordinate error in RPC0 by producing secondary particle. This effect provides a complete explanation for the observed z -distribution differences between experimental and simulated data in Fig. 4a.

To further investigate this phenomenon, simulations with varying roof thicknesses were conducted (specific configurations detailed in Section II). For quantitative analysis of the PoCA point clustering distribution at RPC1’s position, the integral ratio of PoCA point z -coordinates within the [235, 265] mm interval was introduced as an effective metric. This ratio specifically characterizes the proportion of PoCA algorithm reconstructions localized at RPC1. Fig. 5 demonstrates a remarkably strong positive correlation ($R^2 = 0.9753$) between

TABLE I: Lead roof thickness versus PoCA z -coordinate integral ratios (235-265 mm range) from simulations, including the roof-removed configuration. All data obtained with consistent event selection criteria.

Lead roof thickness (mm)	Integral ratio
50	0.283 ± 0.011
25	0.229 ± 0.008
10	0.199 ± 0.007
5	0.161 ± 0.006
0	0.115 ± 0.006

this reconstruction ratio and the thickness of the lead roof shielding. This relationship indicates that the roof’s shielding thickness systematically influences the spatial distribution of reconstructed PoCA points. The complete dataset is recorded in Table I.

The simulation successfully reproduces the experimentally observed distribution shape when the roof thickness is adjusted to 9 mm (Fig. 4b). It should be noted that the simulations don’t calibrate the differences in detection efficiency of RPCs for various particle types (a parameter that is difficult to measure experimentally), resulting in discrepancies between the simulated z -coordinate distribution of the PoCA points at the two detector positions on the edge and the experimental data. Furthermore, as shown in the last row of Table I, merely elevating and expanding the particle generation plane introduces additional factors that lead to a significant increase in the integral ratio, making it doesn’t match the distribution shape shown in Fig. 4b. However, despite these influencing factors, the strong correlation between the roof thickness and the PoCA point distribution at RPC1 remains clearly observable.

V. SUMMARY

The PoCA algorithm typically disregards certain reconstructed points on the detector as noise, but this work reveals they actually originate from a physically meaningful process — the interaction of cosmic ray components (particularly non-muon particles) with both the detector and surrounding materials. The analysis shows that these reconstructed points reflect physical signatures from cosmic ray interactions — specifically, they systematically affect position measurement accuracy through the production of secondary particles. This discovery carries dual significance for muon tomography: first, it establishes that secondary particles from cosmic ray interactions constitute an important factor influencing measurement precision, highlighting the non-negligible impact of non-muon cosmic ray components; second, the strong correlation ($R^2 = 0.9753$) between lead roof thickness and the number of PoCA points on RPC1 reveals an unexpected material discrimination capability, suggesting new approaches for imaging analysis. The findings remind us of revising standard analysis approaches to take these physical effects into consideration in cosmic ray tomography applications.

VI. ACKNOWLEDGEMENTS

This work is supported in part by the National Natural Science Foundation of China under Grants No. 12325504, and No. 12061141002.

VII. DATA AVAILABILITY

All data included in this study are available upon request by contact with the corresponding author.

- ¹K. N. Borozdin, G. E. Hogan, C. Morris, W. C. Priedhorsky, A. Saunders, L. J. Schultz, and M. E. Teasdale, “Radiographic imaging with cosmic-ray muons,” *Nature* **422**, 277 (2003).
- ²G. Bonomi, P. Checchia, M. D’Errico, D. Pagano, and G. Saracino, “Applications of cosmic-ray muons,” *Progress in Particle and Nuclear Physics* **112**, 103768 (2020).
- ³S. Lee, I. Kang, M. Baek, Y. Chung, J. Kang, and Y. Chung, “A new integrated image reconstruction method for muon tomography to improve material identification and image quality,” in *2024 IEEE Nuclear Science Symposium (NSS), Medical Imaging Conference (MIC) and Room Temperature Semiconductor Detector Conference (RTSD)* (IEEE, 2024) p. 1–2.
- ⁴L. He, S.-Y. Luo, X.-M. Liu, Y.-C. Zou, H.-F. Zhang, W.-C. Xiao, Y.-H. Huang, and X.-D. Wang, “Simulation and experimental comparison of the performance of four-corner-readout plastic scintillator muon-detector system,” *Nuclear Science and Techniques* **35** (2024), 10.1007/s41365-024-01530-1.
- ⁵Z. Chen, D. Liu, Y. Wang, D. Han, and H. Gong, “Theoretical time cost to distinguish special nuclear materials in different scenarios through mprctof based muon scattering tomography,” *Nuclear Instruments and Methods in Physics Research Section A: Accelerators, Spectrometers, Detectors and Associated Equipment* **1077**, 170557 (2025).
- ⁶Y. Wang, Y. Fan, X. Wang, and Q. Wen, “Exploration of large angle scattering events for muon tomography,” (2025), 10.2139/ssrn.5119641.
- ⁷Abhishek, R. Karnam, V. Kashyap, and B. Mohanty, “A modular muon telescope for tomography and radiography applications,” *Nuclear Instruments and Methods in Physics Research Section A: Accelerators, Spectrometers, Detectors and Associated Equipment* **1075**, 170399 (2025).
- ⁸P. K. Vinodkumar, E. Avots, C. Ozcinar, and G. Anbarjafari, “3d reconstruction and denoising of high-z materials from muon tomography using 3d cnn,” *Signal, Image and Video Processing* **19** (2025), 10.1007/s11760-025-03992-1.
- ⁹R. López Ruiz, C. Fernández Madrazo, S. Sánchez Cruz, L. Lloret, and P. Martínez Ruiz del Árbol, “Fast simulation for scattering muography applications using generative adversarial neural networks,” (2025), 10.2139/ssrn.5149084.
- ¹⁰S. Luo, H. Zhang, L. Yin, G. Zeng, S. Feng, S. Feng, X. Du, M. Xiao, and X. Wang, “Simulation study on multi-unit integrated muon detection system based on recurrent neural network algorithm,” *Journal of Instrumentation* **20**, P03027 (2025).
- ¹¹X. Yu, Z. Wang, C.-e. Liu, *et al.*, “Proposed peking university muon experiment for muon tomography and dark matter search,” *Physical Review D* **110** (2024), 10.1103/physrevd.110.016017.
- ¹²Q.-T. Li, Y.-L. Ye, W. Ji, C. Wen, H.-T. Liu, and Y.-C. Ge, “A submillimeter spatial resolution achieved by a large sized glass rpc,” *Chinese Physics C* **37**, 016002 (2013).
- ¹³S. Chen, Q. Li, J. Ma, H. Kong, Y. Ye, J. Gao, and Y. Jiang, “Simulation of a small muon tomography station system based on rpcs,” *Journal of Instrumentation* **9**, C10022–C10022 (2014).
- ¹⁴S. Agostinelli, J. Allison, K. Amako, *et al.*, “Geant4—a simulation toolkit,” *Nuclear Instruments and Methods in Physics Research Section A: Accelerators, Spectrometers, Detectors and Associated Equipment* **506**, 250–303 (2003).
- ¹⁵J. Allison, K. Amako, J. Apostolakis, *et al.*, “Geant4 developments and applications,” *IEEE Transactions on Nuclear Science* **53**, 270–278 (2006).
- ¹⁶J. Allison, K. Amako, J. Apostolakis, *et al.*, “Recent developments in geant4,” *Nuclear Instruments and Methods in Physics Research Section A: Accelerators, Spectrometers, Detectors and Associated Equipment* **835**, 186–225 (2016).
- ¹⁷P. Collaboration, “PKMUON_2024: newrpc.yaml configuration file,” https://github.com/PKMuon/PKMUON_2024/blob/text/config/newrpc.yaml.
- ¹⁸R. Brun and F. Rademakers, “Root — an object oriented data analysis framework,” *Nuclear Instruments and Methods in Physics Research Section A: Accelerators, Spectrometers, Detectors and Associated Equipment* **389**, 81–86 (1997).
- ¹⁹C. Hagmann, D. Lange, and D. Wright, “Cosmic-ray shower generator (cry) for monte carlo transport codes,” in *2007 IEEE Nuclear Science Symposium Conference Record* (IEEE, 2007) p. 1143–1146.
- ²⁰S. Lee, I. S. Kang, M. K. Baek, Y. S. Chung, J. Kang, and Y. H. Chung, “Design of a new muon tomography system using a three-layered tacker,” *Nuclear Engineering and Technology* **57**, 103368 (2025).